Full-Color Tuning of Surface Plasmon Resonance by Compositional Variation of Au@Ag Core-Shell Nanocubes with Sulfides

ARTICLE *in* LANGMUIR · FEBRUARY 2012

Impact Factor: 4.46 · DOI: 10.1021/la300154x · Source: PubMed

4 AUTHORS, INCLUDING:

Daeha Seo
University of California, San Francisco
21 PUBLICATIONS **832** CITATIONS

SEE PROFILE

Langmuir

Article

pubs.acs.org/Langmuir

Full-Color Tuning of Surface Plasmon Resonance by Compositional Variation of Au@Ag Core–Shell Nanocubes with Sulfides

Garam Park, Chanhyoung Lee, Daeha Seo, and Hyunjoon Song*

Department of Chemistry, Korea Advanced Institute of Science and Technology, Daejeon 305-701, Korea

Supporting Information

ABSTRACT: In the present study, we demonstrate the precise tuning of surface plasmon resonance over the full visible range by compositional variation of the nanoparticles. The addition of sulfide ions into the Au@Ag core–shell nanocubes generates stable Au@Ag/Ag_2S core–shell nanoparticles at room temperature, and the plasmon extinction maximum shifts to the longer wavelength covering the entire visible range of 500–750 nm. Based on the optical property, the Au@Ag core–shell nanocubes are employed as a colorimetric sensing framework for sulfide detection in water. The detection limit is measured to be 10 ppb by UV–vis spectroscopy and 200 ppb by naked eyes. Such nanoparticles would be useful for decoration and sensing purposes, due to their precise color tunability and high stability.

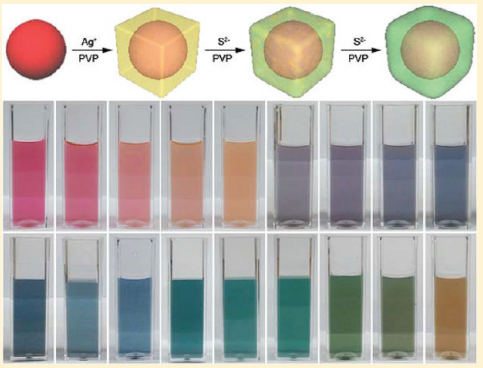

INTRODUCTION

By extreme size reduction approaching a nanometer regime, optical properties of the materials are quite distinct from those of the bulk status.[1,2] For instance, fluorescence at a particular wavelength is a unique feature of semiconducting materials, but nanosize engineering alters the band gap energy and enables full-color tuning of a single component system in the visible range, such as CdSe and CdS.[3]

In case of noble metals, surface plasmon resonance (SPR) dominates optical property and causes very high intensity of extinctions in the visible and near-infrared regions.[4,5] Induced plasmonic dipoles are maximized when conductive objects have the sizes comparable to half of the wavelength of irradiated light, and the resulting extinctions are highly dependent upon morphology (size and shape) of the objects.[6−8] Apparently, there have been several attempts to achieve full-color tuning in the visible region by changing the particle morphology. Plasmonic excitation at a specific wavelength could synthesize uniform Ag nanoprisms with the edge lengths of 40–120 nm, which scattered the light at the wavelength covering a full visible range.[9] Galvanic replacement reactions of Pd or Au on Ag cubes generated hollow nanoboxes, which exhibited continuous extinction spectra from visible to near-infrared regions.[10−12] However, such nanostructures were not much stable under the ambient conditions, because of their highly active structural parts such as sharp tips and rough surfaces.[13,14]

Instead, compositional variation can easily modify optical property of the materials.[15−17] Continuous compositional tuning of InGaN nanowires using a combinatorial chemical vapor deposition approach led to the photoemission varied over the full visible range.[18] In a similar manner, tuning the surface plasmon resonance is expected to be possible through continuous adjustment of dielectric constants in noble metal systems.

One of the most successful applications in plasmonic nanostructures is the high sensitive detection of molecules.[7,19] The SPR wavelengths appreciably shift by slight change of the morphology[13] or surrounding refractive index[20,21] of the metal nanostructures, and thus well-defined metal structures can be used as sensitive colorimetric indicators.

In this study, we present a potential system for the precise full-color tuning of surface plasmon resonance by simple chemical treatment. The addition of sulfide ions to well-defined Au@Ag core–shell nanocubes generates Ag_2S layers on the surface and shifts the extinction maximum to the longer wavelength. Continuous variation of the sulfur concentration yielded colloidal dispersions of the Au@Ag/Ag_2S nanoparticles with intense extinctions over the full visible ranges of 500–750 nm. The particles are very stable and maintain their color for a long time under an ambient condition. This nanoparticle system behaves as a useful framework for colorimetric sensing of sulfide ions in an aqueous solution with the sensitivity up to 10 ppb.

EXPERIMENTAL SECTION

Reagents. Tetrachloroaurate trihydrate ($HAuCl_4 \cdot 3H_2O$, 99.9+%, Aldrich), silver nitrate ($AgNO_3$, 99+%, Aldrich), poly(vinylpyrrolidone) (PVP, M_w = 55 000, Aldrich), 1,5-pentanediol (PD, 96%, Aldrich), diethylene glycol (DEG, 99%, Aldrich), sodium

Special Issue: Colloidal Nanoplasmonics

Received: January 11, 2012
Revised: February 3, 2012

   dx.doi.org/10.1021/la300154x | Langmuir XXXX, XXX, XXX–XXX

Scheme 1. Synthesis of Au@Ag/Ag_2S Core−Shell Nanoparticles

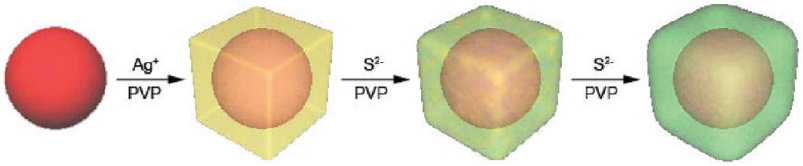

sulfide nonahydrate ($Na_2S·9H_2O$, 99.99+%, Aldrich), and nitric acid (HNO_3, 60−61%, Junsei) were used as received.

Synthesis of Au Spherical Seeds. The synthesis was performed according to the literature.[22] A $AgNO_3$ solution in PD (0.30 mL, 0.020 M) was added to boiling PD (40 mL). Then, PVP (12 mL, 0.15 M) and $HAuCl_4$ (6.0 mL, 0.050 M) solutions in PD were periodically added every 30 s over 7.5 min. The resulting mixture was refluxed for 1 h. The product was purified by a repetitive dispersion/precipitation cycle with ethanol and was finally dispersed in ethanol (30 mL) for further reactions.

Synthesis of Au@Ag Core−Shell Nanocubes with Different Shell Thicknesses. The gold seed dispersion in DEG (1.0 mL, 0.075 M with respect to the gold precursor concentration), PVP (0.75 mL, 0.30 M), nitric acid (7.5 μmol), and $AgNO_3$ (0.75 mL, 0.10 M) solutions in DEG were added to DEG (6.0 mL) at 160 °C. The mixture was stirred at the same temperature for 1 h. The product was washed with ethanol by a repetitive precipitation/dispersion cycle. The particles were finally collected by centrifugation and dispersed in distilled water (30 mL). By changing the volume (0.5−2.0 mL) of the gold seed dispersion in the identical procedure, the Au@Ag core−shell nanocubes with different shell thicknesses were yielded.

Modification of Au@Ag Core−Shell Nanocubes with Sulfide Ions. The aqueous dispersion of the Au@Ag core−shell nanocubes (5.0 mL, 0.44 mM with respect to the Ag precursor concentration) was mixed with an aqueous solution of Na_2S at room temperature. A different amount of Na_2S (from 0.44 μmol, 0.2 equiv to 0.022 mmol, 10 equiv with respect to the Ag precursor concentration) was used for the precise composition control. The mixture was stirred in a vial exposed in air for 6 h. The products were centrifuged and washed three times with deionized water to remove residual impurities.

Colorimetric Sensing of Sulfide Ions. The Au@Ag core−shell nanoparticles (3.6×10^{-9} ea) were dispersed in deionized water (2.0 mL). A small amount of Na_2S (from 2.2 nmol, 0.01 equiv to 11 nmol, 0.05 equiv) was added to the particle dispersion, and the mixture was allowed to stir at room temperature. The resulting dispersion was measured by UV−vis spectroscopy.

Characterization. SEM images were obtained using a Philips XL30S FEG operated at 10 kV. Transmission electron microscopy (TEM) and high resolution TEM (HRTEM) images, selected area electron diffraction (SAED) patterns, energy dispersive X-ray spectroscopy (EDX) spectra, and line profiles were acquired on a JEOL FB-2100F (HR) instrument operated at 200 kV at National Nanofabrication Center at KAIST. X-ray diffraction (XRD) patterns were recorded on a Rigaku D/max-IIIC (3 kW) diffractometer using Cu Kα radiation. The samples were prepared by a few drops of the colloidal solutions in ethanol either on copper grids coated with lacey carbon film (Ted Pella, Inc.) for TEM, on small pieces (5 mm × 5 mm) of silicon wafer (P-100) for SEM, or on small pieces (1 cm × 1 cm) of slide glass for XRD, and were allowed to dry in air. The UV−vis absorption data were recorded on a Jasco V670 UV−vis-NIR spectrophotometer using aqueous colloidal dispersions.

RESULTS AND DISCUSSION

The overall synthetic scheme of the Au@Ag/Ag_2S core−shell nanoparticles is depicted in Scheme 1. The Au@Ag core−shell nanocubes were synthesized according to the literature.[22,23] The average diameter of the Au spherical seeds is estimated to be 53 ± 7 nm. By using different amounts of the Au seeds with the $AgNO_3$ solution, the average edge size of the Au@Ag nanoparticles varies from 59 ± 8 to 62 ± 9 and 67 ± 13 nm, and the morphology changes from truncated to perfect and overgrown cubes, respectively (Supporting Information, Figure S1).

The addition of sulfide ions into the Au@Ag core−shell nanocubes suddenly changes the dispersion color from yellow orange to violet (vide infra). Basically, the sulfide ions react with metallic Ag and generate Ag_2S in air at room temperature as follows.[24−27]

$$4Ag + 2S^{2-} + O_2 + 2H_2O \rightarrow 2Ag_2S + 4OH^-$$

The resulting Ag_2S layer formation on the surface of the Au@Ag nanocubes alters the refractive index from Ag ($n_{Ag} \sim 0.05$) to Ag_2S ($n_{Ag2S} \sim 2.9$) in the visible range, which largely changes surface plasmon extinction of the particle dispersion.[28,29]

To demonstrate, we have measured each of the sample dispersions by UV−vis spectroscopy (Figure 1a). The original Au seed dispersion is red-colored, with the peak maximum at 525 nm (red line). By increasing the Ag shell thickness, the surface plasmon extinction continuously shifts to the lower wavelength down to 511 nm, along with the color change from red to yellow orange (Figure 1b). These blue-shifts are attributed to the refractive index close to that of the bulk Ag, by continuous surface growth of the Ag component.[23,30,31] The sample in the fourth cuvette of Figure 1b is referred to as **A**, which is composed of the Au@Ag core−shell nanocubes with the average edge size of 62 ± 9 nm (Supporting Information, Figure S1b).

A different amount of sulfide ions from 0.2 to 10 equiv with respect to the original silver precursor concentration was added to the sample **A**, and the mixture was stirred in an aerial condition for 6 h. The dispersion color shifts to violet (the first cuvette in Figure 1c) with the extinction centered at 555 nm, when 0.2 equiv of the sulfide ions was added. Then, the color continuously changes from violet to green, and the extinction peak shifts to 668 nm, along with the increment of sulfide loading. When the 0.5, 1.0, 4.0, and 10 equiv of the sulfide ions are added to the particle dispersion, the extinction maximum shifts to 579 (dark blue), 617 (blue), 639 (bluish green), and 668 (green) nm, where the samples are referred to as **B**, **C**, **D**, and **E**, respectively, as depicted in Figure 1. The prolonged reactions with excess sulfide ions for 3 and 10 days exhibit further shifts of the extinction peaks up to 720 (yellow green) and 783 (yellow brown) nm, respectively, as in the last two cuvettes of Figure 1c. However, the extinction peaks are broad, presumably due to the irregular deposition of sulfides.

The sample **E** was characterized by various TEM-based measurements. The particles are uniform in shape with the average edge size of 70 ± 16 nm (Supporting Information, Figure S2). The high angle annular dark field-scanning transmission electron microscopy (HAADF-STEM) and TEM images (Figure 2a,b) show that each particle has a spherical Au core and a thin shell with a rough surface deviated from the perfect cubic shape. The inset is the selective area electron

dx.doi.org/10.1021/la300154x | Langmuir XXXX, XXX, XXX−XXX

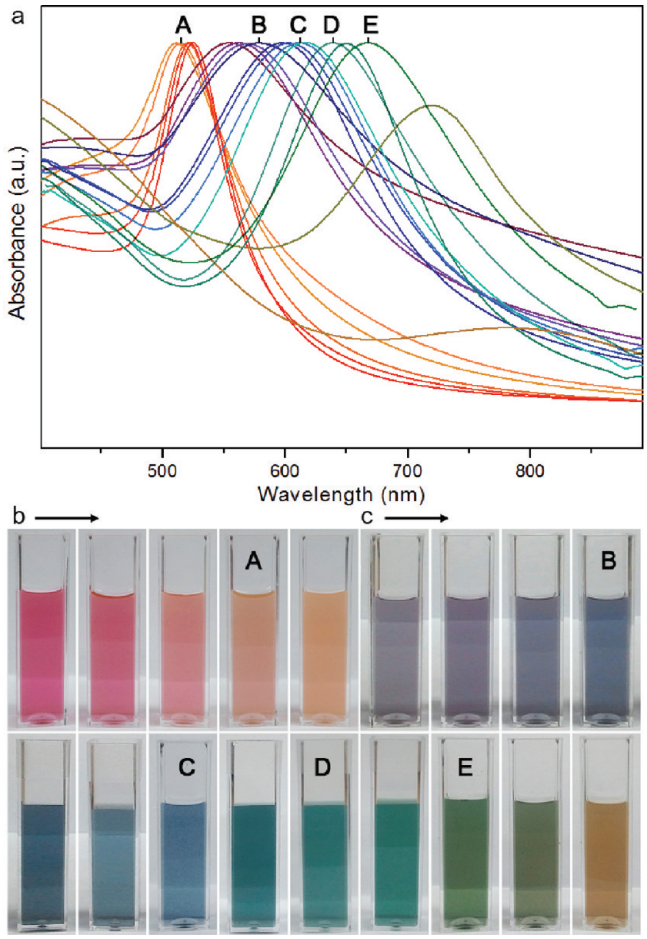

Figure 1. Surface plasmon resonance shifts of Au seeds, Au@Ag core–shell nanocubes, and Au@Ag/Ag_2S nanoparticles. (a) UV–vis absorption spectra. Photographs of the aqueous dispersions of (b) Au seeds and Au@Ag core–shell nanocubes, and (c) Au@Ag/Ag_2S nanoparticles. The representative samples are referred to as **A** (orange), **B** (dark blue), **C** (blue), **D** (bluish green), and **E** (green).

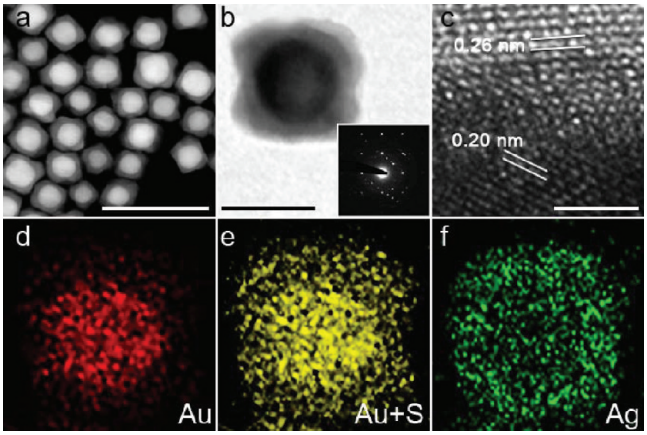

Figure 2. (a) HAADF-STEM and (b) TEM images, (b inset) SAED pattern, and (c) HRTEM image of a single nanoparticle of the sample **E**. Elemental mapping of (d) Au at 2.120 keV, (e) both Au and S at 2.307 keV, and (f) Ag at 2.984 keV. The bars represent (a) 200 nm, (b) 50 nm, and (c) 2 nm.

diffraction (SAED) pattern, which comprises both a cubic pattern originated from the face-centered cubic Au core and a pattern from the monoclinic Ag_2S. The intense spots neighbored to the center are assigned to be Au(200), Ag_2S(200), Ag_2S(−121), and Ag_2S(−112). The HRTEM image of the interface between core and shell regions (Figure 2c) indicates that the core is single crystalline with the lattice fringe distance of 0.20 nm, assigned to that of the Au(200) planes, and the shell is polycrystalline with the lattice fringe distance of 0.26 nm, corresponding to that of the Ag_2S(−121) planes, respectively. EDX analysis estimated the elemental fractions of Au, Ag, and S to be 32, 46, and 22%, respectively. The ratio of S and Ag is nearly 1:2, although the Au Mα and S Kα peaks are partially overlapped, indicating that the particles are composed of Au and Ag_2S. The elemental mapping in Figure 2d–f indicates that there is no alloy formation between Au and Ag, and the particle has a Au core with a shell containing both Ag and S. The line profile analysis along a diagonal line of the single particle shows typical trajectories of the Au and Ag components on the core–shell structure (Supporting Information, Figure S3). These data confirm that the sample **E** comprises the Au@Ag_2S core–shell nanoparticles.

There were several reports on the Au@Ag_2S core–shell nanostructures thus far. Guyot-Sionnest and Liu, and Shen et al. demonstrated Ag_2S coating on Au nanorods, which exhibited large red-shifts of the surface plasmon resonance.[24,25] Ying and Yang also reported the isotropic deposition of Ag_2S onto the Au seeds.[32] The structural and compositional features of these materials are consistent well with the sample **E**. The values of red-shift in the UV–vis spectra are distinct in all nanostructures, due to high sensitivity of the surface plasmon resonance on the shape and thickness of the Ag_2S shells and the Au cores.

The samples **B** to **D** were also characterized by TEM, XRD, and EDX. By the addition of sulfide ions, a bump was formed at one side of the Ag shell in **B**, more bumps appeared in **C** and **D**, and the bumps covered the entire surface in **E** (Figure 3a). These result from the formation of polycrystalline Ag_2S domains in the Ag shells. Under the present reaction conditions at room temperature, the reaction with sulfide ions was begun at some active surface sites such as defects or kinks. The volume of one Ag_2S unit is 67% larger than that of two Ag atoms by the incorporation of S^{2-}, and thus the shell expands outward to form irregular bumps at specific points. The Au cores were sufficiently inert and maintained their spherical morphology during the sulfidation reaction. Such continuous change from Ag to Ag_2S on the shells adjusted the average environment (or refractive index) around the Au cores, and shifted surface plasmon resonance to the longer wavelength.

The XRD spectra demonstrate compositional and structural variations of the sample **A**-**E** (Figure 3b). The distinctive peaks at 30–35°, assignable to the (−112), (−121), and (022) reflections of monoclinic Ag_2S (JCPDS No. 14-0072), are not observable in **B** and **C**, but appear in **D** and **E**, because of the detection limit in the XRD measurement. The intense (111), (200), and (220) reflections are characteristic signals of the face-centered cubic Au (JCPDS No. 04-0784) and appear in all samples. Interestingly, the relative peak intensity ratio of (111)/(200) continuously increases from **A** to **E**.[33] **A** has the ratio of 0.28, indicative of simultaneous alignment of the nanoparticles along {100} planes normal to the substrate, due to their perfect cubic morphology, as observed in Au and Ag cubes. Through **B** and **C**, the ratio does not change a lot, because the outer Ag shells are not much deviated from the cubic shape. However, the shells contain many bumps in **D**, and the cubic symmetry is entirely broken in **E**. The particle alignment is nearly random in

dx.doi.org/10.1021/la300154x | *Langmuir* XXXX, XXX, XXX–XXX

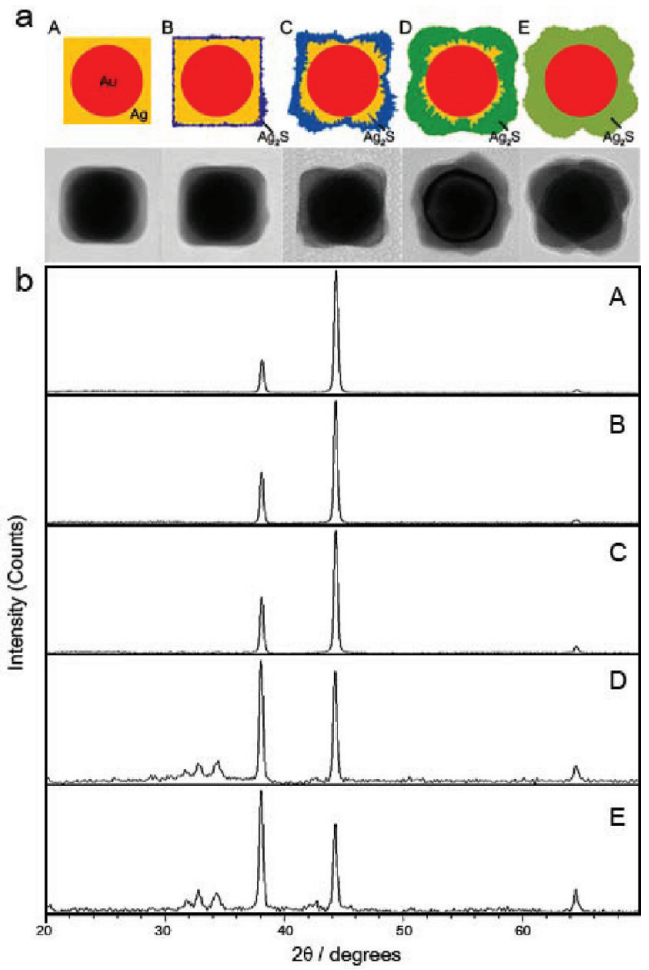

Figure 3. (a) Structural schemes and TEM images of individual particles, and (b) XRD spectra for **A**–**E**.

E, and the ratio (1.38) reaches that of either the spherical particles or the bulk materials.

The EDX analysis of the sample **A**–**E** was performed (Supporting Information, Figure S4). The S/Ag composition ratios are estimated to be 0, 0.10, 0.27, 0.38, and 0.47 for samples **A**–**E**, respectively. If we consider the conversion yield of Ag to Ag_2S by the addition of sulfides, the structures can be formulated to be the Au@(1-x)Ag/(x/2)Ag_2S core–shell nanoparticles, with x = 0, 0.2, 0.54, 0.76, and 0.94, respectively.

As shown in Figure 1, the peak maximum of surface plasmon resonance shifts to the longer wavelength from **A** to **E**, and the dispersion color covers the entire visible range. As the S/Ag composition ratio of the particles increases, the peak maximum (λ_{max}) monotonically shifts to the red region, but not linearly (Figure 4a). It is known that the surface plasmon extinction maximum is in proportional to the dielectric constant (or refractive index in some literature) of surroundings on the metal surface.[4,34−36] We have investigated the sensitivity of the Au@Ag core–shell nanocubes and the Au spherical seeds on the solvents with different refractive indices (water (1.33), ethanol (1.36), isopropanol (1.38), ethylene glycol (1.44), and tetraethylene glycol (1.46)), and observed linear relationships between the solvent refractive index and the peak maximum for both particles (Figure 4b). The sensitivity factors are estimated to be 184 and 119 nm RIU^{-1} for the Au@Ag nanocubes and the Au spheres, respectively. The former is larger due to high sensitivity of the Ag surface compared to that of Au. Based on these experiments, the nonlinear increment of the λ_{max} compared to the S/Ag ratio can be elucidated. **A** has the outer Ag surface, which is more sensitive to the environmental change, and thus shows large sensitivity, whereas **E** has the conductive part similar to the Au sphere, leading to less sensitivity toward the refractive index change from Ag to Ag_2S. As the Ag_2S component grows from **A** to **E**, the Ag component of the shells diminishes, and the conductive part shrinks to the Au cores, which causes lowering the sensitivity, as shown in Figure 4a.

The Ag nanocubes without the Au cores also change their colors by the addition of sulfide ions (Supporting Iinformation, Figure S5).[37,38] When a tiny amount of sulfide ions was added, the Ag@Ag_2S core–shell nanoparticles were successfully formed, with an abrupt shift of the surface plasmon to the red region.[26] However, the reaction did not occur uniformly, and the particles were readily degraded by the continuous addition of sulfides. On the other hand, in the Au@Ag/Ag_2S nanoparticles, the Au cores are inert against severe sulfidation conditions and prevent rapid degradation of the particle structure. The Au@Ag core–shell nanocube synthesis is

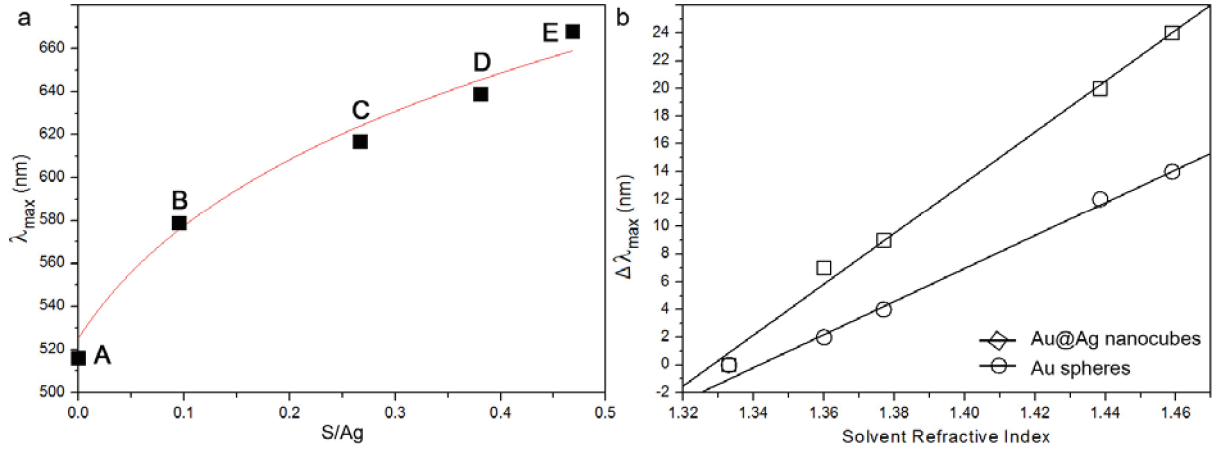

Figure 4. (a) Relationship of the S/Ag molar ratio analyzed by EDX versus surface plasmon peak maximum (λ_{max}). (b) Sensitivity factors (refractive index versus peak maximum change) of the Au@Ag nanocubes (□) and the Au spherical seeds (○) dispersed in five different solvents (water, ethanol, isopropanol, ethylene glycol, and tetraethylene glycol).

dx.doi.org/10.1021/la300154x | *Langmuir* XXXX, XXX, XXX–XXX

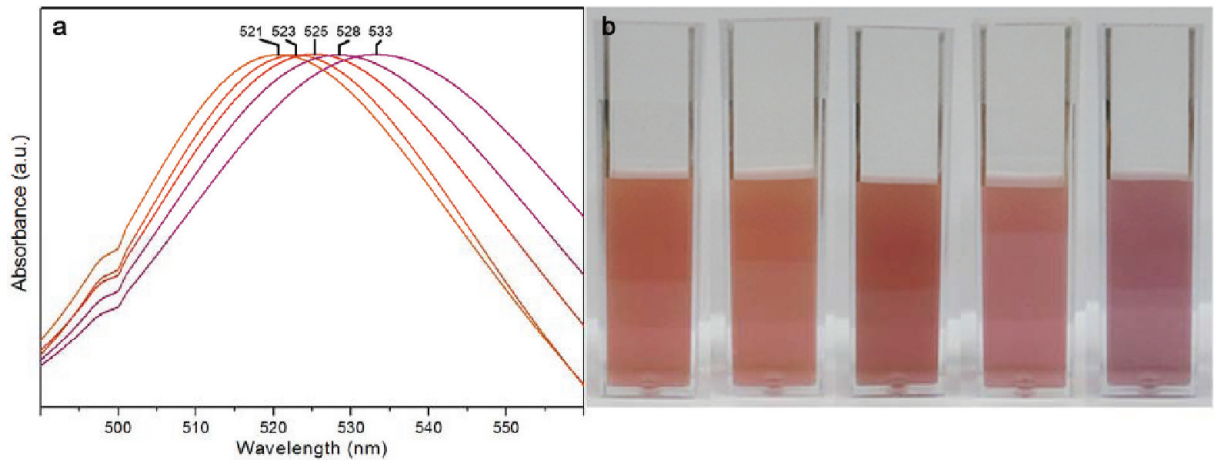

Figure 5. (a) UV−vis spectra of 3.6×10^9 Au@Ag core−shell nanocubes dispersed in 2.0 mL of deionized water. 0.01−0.05 equiv of sulfides with respect to the Ag content was introduced. (b) Photographs of the cuvettes with 4-fold concentrated dispersions.

basically through the seed-mediated process, which provides consistent and large scale synthesis up to a gram scale without loss of particle uniformity.

The Au@Ag/Ag_2S nanoparticles are very stable in the form of the particles themselves as well as aqueous dispersions under an ambient condition. The samples **A**−**E** as aqueous dispersions were stored in cuvettes for 40 day, and there were no observable changes such as colors and particle aggregation of the samples (Supporting Information, Figure S6).

The Au@Ag core−shell nanocubes seem to be useful as a novel framework for colorimetric sensing of various elements.[35,39−45] Thus far, we have shown precise color tuning of the particle dispersion by the addition of sulfide ions. It means that the Au@Ag nanocubes can detect the sulfide ions in an aqueous solution by color change. To demonstrate, 3.6×10^9 Au@Ag core−shell nanocubes were dispersed in 2.0 mL of deionized water. The sulfide ions were added to the dispersion, and the extinction was monitored using UV−vis spectroscopy. Figure 5a shows the surface plasmon extinctions of the particle dispersions where 2.2, 4.4, 6.6, 8.8, and 11×10^{-9} mol (0.01, 0.02, 0.03, 0.04, and 0.05 equiv with respect to the Ag content of the particles) were added. The original Au@Ag core−shell nanocubes have the peak maximum at 516 nm, and the peak shifts to 521, 523, 525, 528, and 533 nm by the sulfide addition, respectively. The detection limit of the UV−vis spectrometer is 1.0 nm; therefore, 6.5×10^{-10} mol or 10 ppb detection can be achieved.[40] Figure 5b shows the dispersion colors corresponding to the samples in Figure 5a with 4-fold concentrations. The colors of the first, third, and fifth cuvettes are distinguishable, indicating that the detection limit is ∼5 nm, and 200 ppb of the sulfide ions in aqueous solutions are detectable by naked eyes. If the individual particles can be measured using single particle spectroscopy, the detection limit is calculated to be 180 zmol, which is comparable to ∼100 zmol detection using a single Ag nanocube reported by Van Duyne and McFarland.[41]

The gold and silver nanoparticles have been used as stable pigments for stained-glass arts since the middle age. In order to confirm usefulness of the Au@Ag/Ag_2S core−shell nanoparticles as solid pigments, three samples, gold nanoparticles, **D**, and **C**, were selected for the representative colors of red, green, and blue, respectively (Figure 6a). The concentration of aqueous dispersions was adjusted to obtain an optical density of 1.0 at the peak maximum (Figure 6b). Three common organic

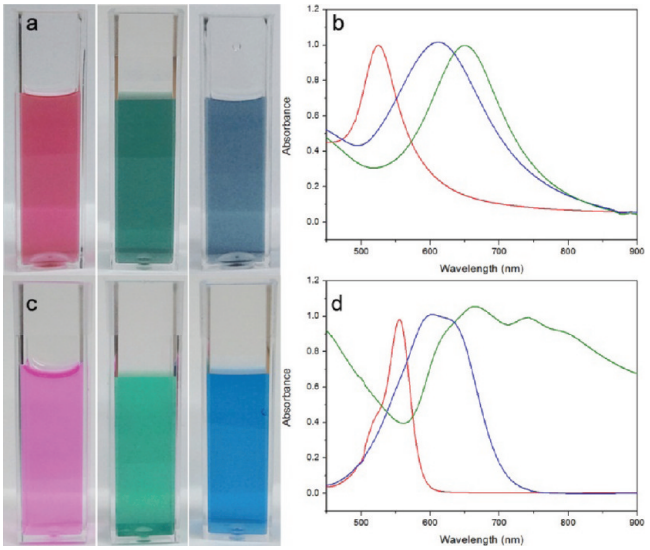

Figure 6. (a) Photographs and (b) UV−vis spectra of aqueous dispersions of gold nanoparticles (red), sample **D** (green), and **C** (blue). (c) Photographs and (d) UV−vis spectra of aqueous solutions of rhodamine B isothiocyanate (red), pigment green 7 (green), and acid blue 25 (blue). The concentrations of the particles and organic dyes were adjusted to obtain the optical densities at the peak maxima of 1.0.

dyes, including rhodamine B isothiocyanate (RBITC, red), pigment green 7 (green), and acid blue 25 (blue), were also selected for comparison, with the optical density of 1.0 at the peak maximum (Figure 6c,d). The nanoparticles and organic dyes exhibit similar features of the UV−vis spectra, in terms of peak broadness and solution stability. Interestingly, the costs of gold nanoparticles and the samples **D** and **C** used in this experiment are economically competitive to those of organic dyes. For instance, the amount of the gold nanoparticles used in Figure 6a is 4.0×10^{-7} mol with respect to the gold precursor concentration, and the total cost is estimated to be $0.018, whereas the amount of RBITC is 5.3×10^{-8} mol with the cost of $0.040. The cost of the Au@Ag/Ag_2S core−shell nanoparticles is estimated to be $0.010, which is cheaper than the gold nanoparticles, due to the existence of Ag and S components.

dx.doi.org/10.1021/la300154x | *Langmuir* XXXX, XXX, XXX−XXX

The Au@Ag/Ag_2S core−shell nanoparticles are also useful to be incorporated as pigments into the films. The Au@Ag/Ag_2S nanoparticles dispersed in 2-propanol were mixed with Sylgard 184, and the mixture was casted on the substrate to yield polydimethylsiloxane (PDMS) color films. Because the refractive index of PDMS (1.42) is larger than that (1.33) of water, the extinction of each sample shifts to the longer wavelength. Therefore, we have adjusted the sulfur loading amounts of the nanoparticles and generated red, green, and blue PDMS films, as shown in Figure 7. The nanoparticle dyes

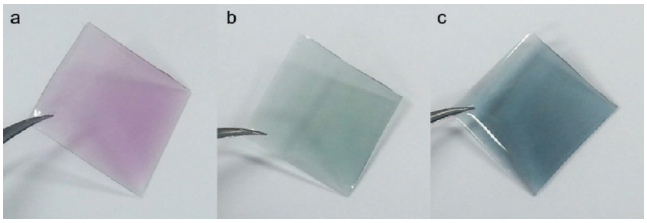

Figure 7. Formation of (a) red, (b) green, and (c) blue PDMS films using Au@Ag/Ag_2S core−shell nanoparticles.

were evenly dispersed in the PDMS matrices, and the resulting films were sufficiently stable during the curing process at 60 °C for 12 h.

In summary, full-color tuning of surface plasmon extinctions in the visible range was achieved by the continuous addition of sulfide ions into the Au@Ag core−shell nanocubes. The sulfide ions reacted with the Ag shells and generated Ag_2S, forming stable Au@$(1 - x)$Ag/$(x/2)Ag_2S$ core−shell nanoparticles, and the particle dispersions showed the surface plasmon resonances covering the entire visible range. The nanoparticles were employed as a framework for colorimetric sensing of the sulfide ions in aqueous solutions, with the detection limit of 10 ppb by UV−vis spectroscopy and 200 ppb by naked eyes. These particles with various colors (or extinctions) would be valuable as solid pigments for decorations and filters, and also be useful as a stable colorimetric sensing framework for the detection of molecules, such as heavy metal ions and biomolecules.

■ ASSOCIATED CONTENT

Supporting Information

Additional characterization data of the sample **A**−**E** and the Ag nanocubes. This material is available free of charge via the Internet at http://pubs.acs.org.

■ AUTHOR INFORMATION

Corresponding Author

*E-mail: hsong@kaist.ac.kr.

Notes

The authors declare no competing financial interest.

■ ACKNOWLEDGMENTS

This work was supported by the Core Research Program (2010-07592) and the Pioneer Research Program (2008-05103) through the National Research Foundation of Korea funded by the Ministry of Education, Science, and Technology.

■ REFERENCES

(1) Brongersma, M. L.; Shalaev, V. M. The Case for Plasmonics. *Science* **2010**, *328*, 440−441.
(2) Alivisatos, A. P. Semiconductor Clusters, Nanocrystals, and Quantum Dots. *Science* **1996**, *271*, 933−937.
(3) Murray, C. B.; Norris, D. J.; Bawendi, M. G. Synthesis and characterization of nearly monodisperse CdE (E = sulfur, selenium, tellurium) semiconductor nanocrystallites. *J. Am. Chem. Soc.* **1993**, *115*, 8706−8715.
(4) Bohrenm, C. F.; Huffman, D. R. *Absorption and Scattering of Light by small particles*; John Wiley and Sons, Inc.: New York, 1983.
(5) Maier, S. A. *Plasmonics: Fundamentals and Applications*; Springer: New York, 2007.
(6) Link, S.; El-Sayed, M. A. Optical Properties and Ultrafast Dynamics of Metallic Nanocrystals. *Annu. Rev. Phys. Chem.* **2003**, *54*, 331−366.
(7) Rycenga, M.; Cobley, C. M.; Zeng, J.; Li, W.; Moran, C. H.; Zhang, Q.; Qin, D.; Xia, Y. Controlling the Synthesis and Assembly of Silver Nanostructures for Plasmonic Applications. *Chem. Rev.* **2011**, *111*, 3669−3712.
(8) Halas, N. J.; Lal, S.; Chang, W.; Link, S.; Nordlander, P. Plasmons in Strongly Coupled Metallic Nanostructures. *Chem. Rev.* **2011**, *111*, 3913−3961.
(9) Jin, R.; Cao, Y.; Mirkin, C. A.; Kelly, K. L.; Schatz, G. C.; Zheng, J. G. Photoinduced Conversion of Silver Nanospheres to Nanoprisms. *Science* **2001**, *294*, 1901−1903.
(10) Sun, Y.; Xia, Y. Mechanistic Study on the Replacement Reaction between Silver Nanostructures and Chloroauric Acid in Aqueous Medium. *J. Am. Chem. Soc.* **2004**, *126*, 3892−3901.
(11) Chen, J.; Wiley, B.; McLellan, J.; Xiong, Y.; Li, Z.-Y.; Xia, Y. Optical Properties of Pd-Ag and Pt-Ag Nanoboxes Synthesized via Galvanic Replacement Reactions. *Nano Lett.* **2005**, *5*, 2058−2062.
(12) González, E.; Arbiol, J.; Puntes, V. F. Carving at the Nanoscale: Sequential Galvanic Exchange and Kirkendall Growth at Room Temperature. *Science* **2011**, *334*, 1377−1380.
(13) Zeng, J.; Robert, S.; Xia, Y. Nanocrystal-Based Time-Temperature Indicators. *Chem.—Eur. J.* **2010**, *16*, 12559−12563.
(14) Zhang, Q.; Ge, J.; Pham, T.; Goebl, J.; Hu, Y.; Lu, Z.; Yin, Y. Reconstruction of Ag Nanoplates by UV Irradiation: Tailored Optical Property and Enhanced Stability. *Angew. Chem., Int. Ed.* **2009**, *48*, 3516−3519.
(15) Zhang, K.; Xian, Y.; Wu, Z.; Feng, L.; He, W.; Liu, J.; Zhou, W.; Xie, S. Enhanced Optical Responses of Au@Pd Core/Shell Nanobars. *Langmuir* **2009**, *25*, 1162−1168.
(16) Liu, M. Z.; Guyot-Sionnest, P. Synthesis and Optical Characterization of Au/Ag Core/Shell Nanorods. *J. Phys. Chem. B* **2004**, *108*, 5882−5888.
(17) Zhang, J.; Tang, Y.; Weng, L.; Ouyang, M. Versatile Strategy for Precisely Tailored Core@Shell Nanostructures with Single Shell Layer Accuracy: The Case of Metallic Shell. *Nano Lett.* **2009**, *9*, 4061−4065.
(18) Kuykendall, T.; Ulrich, P.; Aloni, S.; Yang, P. Complete composition tenability of InGaN nanowires using a combinatorial approach. *Nat. Mater.* **2007**, *6*, 951−956.
(19) Rosi, N. L.; Mirkin, C. A. Nanostructures in Biodiagnostics. *Chem. Rev.* **2005**, *105*, 1547−1562.
(20) Anker, J. N.; Hall, W. P.; Lyandres, O.; Shah, N. C.; Zhao, J.; Van Duyne, R. P. Biosensing with plasmonic nanosensors. *Nat. Mater.* **2008**, *7*, 442−453.
(21) Stewart, C. R.; Anderton, M. E.; Thompson, L. B.; Maria, J.; Gray, S. K.; Rogers, J. A.; Nuzzo, R. G. Nanostructured Plasmonic Sensors. *Chem. Rev.* **2008**, *108*, 494−521.
(22) Seo, D.; Park, J. C.; Song, H. Polyhedral Gold Nanocrystals with O_h Symmetry: From Octahedra to Cubes. *J. Am. Chem. Soc.* **2006**, *128*, 14863−14870.
(23) Park, G.; Seo, D.; Jung, J.; Ryu, S.; Song, H. Shape Evolution and Gram-Scale Synthesis of Gold@Silver Core-Shell Nanopholyhedrons. *J. Phys. Chem. C* **2011**, *115*, 9417−9423.
(24) Liu, M.; Guyot-Sionnest, P. Preparation and optical properties of silver chalcogenide coated gold nanorods. *J. Mater. Chem.* **2006**, *16*, 3942−3945.

(25) Zhu, J.; Shen, Y.; Xie, A.; Zhu, L. Tunable surface plasmon resonance of Ag@Ag_2S core-shell nanostructures containing voids. *J. Mater. Chem.* **2009**, *19*, 8871−8875.
(26) Zeng, J.; Tao, J.; Su, D.; Zhu, Y.; Qin, D.; Xia, Y. Selective Sulfuration at the Corner Sites of a Silver Nanocrystal and It use in Stabilization of the Shape. *Nano Lett.* **2011**, *11*, 3010−3015.
(27) Levard, C.; Reinsch, B.; Michel, F. M.; Oumahi, C.; Lowry, G. V.; Brown, G. E. Jr. Sulfidation Processes of PVP-Coated Silver Nanoparticles in Aqueous Solution: Impact on Dissolution Rate. *Environ. Sci. Technol.* **2011**, *45*, 5260−5266.
(28) Johnson, P. B.; Christy, R. W. Optical Constants of the Noble Metals. *Phys. Rev. B* **1972**, *6*, 4370−4379.
(29) Bennett, J. M.; Stanford, J. L.; Ashley, E. J. Optical Constants of Silver Sulfide Tarnish Films. *J. Opt. Soc. Am.* **1970**, *60*, 224−232.
(30) Liz-Marzán, L. M. Tailoring Surface Plasmons through the Morphology and Assembly of Metal Nanoparticles. *Langmuir* **2006**, *22*, 32−41.
(31) Gonzalez, C. M.; Liu, Y.; Scaiano, J. C. Photochemical Strategies for the Facile Synthesis of Gold-Silver Alloy and Core-Shell Bimetallic Nanoparticles. *J. Phys. Chem. C* **2009**, *113*, 11861−11867.
(32) Yang, J.; Ying, J. Y. Room-temperature synthesis of nanocrystalline Ag_2S and its nanocomposites with gold. *Chem. Commun.* **2009**, 3187−3189.
(33) Sun, Y.; Xia, Y. Shape-Controlled Synthesis of Gold and Silver Nanoparticles. *Science* **2002**, *298*, 2176−2179.
(34) Jensen, T. R.; Duval, M. L.; Kelly, K. L.; Lazarides, A. A.; Schatz, G. C.; Van Duyne, R. P. Nanosphere Lithography: Effect of the External Dielectric Medium on the Surface Plasmon Resonance Spectrum of a Periodic Array of Silver Nanoparticles. *J. Phys. Chem. B* **1999**, *103*, 9846−9853.
(35) Mayer, K. M.; Hafner, J. H. Localized Surface Plasmon Resonance Sensors. *Chem. Rev.* **2011**, *111*, 3828−3857.
(36) Chen, H.; Kou, X.; Yang, Z.; Ni, W.; Wang, J. Shape- and Size-Dependent Refractive Index Sensitivity of Gold Nanoparticles. *Langmuir* **2008**, *24*, 5233−5237.
(37) Pang, M.; Hu, J.; Zeng, H. C. Synthesis, Morphological Control, and Antibacterial Properties of Hollow/Solid Ag_2S/Ag Heterodimers. *J. Am. Chem. Soc.* **2010**, *132*, 10771−10785.
(38) Kryukov, A. I.; Stoyuk, A. L.; Zin'chuk, N. N.; Korzhak, A. V.; Kuchmii, S. Ya. Optical and catalytic properties of Ag_2S nanoparticles. *J. Mol. Catal. A* **2004**, *221*, 209−221.
(39) Rex, M.; Hernandez, F. E.; Campiglia, A. D. Pushing the Limits of Mercury Sensors with Gold Nanorods. *Anal. Chem.* **2006**, *78*, 445−451.
(40) Forzani, E. S.; Foley, K.; Westerhoff, P.; Tao, N. Detection of arsenic in groundwater using a surface plasmon resonance sensor. *Sens. Actuators, B* **2007**, *123*, 82−88.
(41) McFarland, A. D.; Van Duyne, R. P. Single Silver Nanoparticles as Real-Time Optical Sensors with Zeptomole Sensitivity. *Nano Lett.* **2003**, *3*, 1057−1062.
(42) Kim, J.-Y.; Lee, J.-S. Synthesis and Thermodynamically Controlled Anisotropic Assembly of DNA-Silver Nanoprism Conjugates for Diagnostic Applications. *Chem. Mater.* **2010**, *22*, 6684−6691.
(43) Nath, N.; Chilkoti, A. A Colorimetric Gold Nanoparticle Sensor To Interrogate Biomolecular Interactions in Real Time on a Surface. *Anal. Chem.* **2002**, *74*, 504−509.
(44) Nusz, G. J.; Curry, A. C.; Marinakos, S. M.; Wax, A.; Chilkoti, A. Rational Selection of Gold Nanorod Geometry for Lable-Free Plasmonic Biosensors. *ACS Nano* **2009**, *3*, 795−806.
(45) Hall, W. P.; Ngatiz, S. N.; Van Duyne, R. P. LSPR Biosensor Signal Enhancement Using Nanoparticle-Antibody Conjugates. *J. Phys. Chem. C* **2011**, *115*, 1410−1414.